ChemComm

COMMUNICATION

View Article Online
View Journal

Cite this: DOI: 10.1039/c6cc02698b

Received 31st March 2016,
Accepted 26th June 2016

DOI: 10.1039/c6cc02698b

www.rsc.org/chemcomm

Structures and magnetism of mono-palladium and mono-platinum doped $Au_{25}(PET)_{18}$ nanoclusters†

Shubo Tian,[a] Lingwen Liao,[a] Jinyun Yuan,[b] Chuanhao Yao,[a] Jishi Chen,[a] Jinlong Yang[b] and Zhikun Wu*[a]

Herein we report three important results of widespread interest, which are (1) the crystal structure of $[Au_{24}Pt(PET)_{18}]^0$, (2) the crystal structure of $[Au_{24}Pd(PET)_{18}]^0$ and (3) the main source of magnetism in $[Au_{25}(PET)_{18}]^0$.

Doped metal nanoparticles have attracted extensive attention for many years due to their intriguing properties and promising applications in a wide range of fields such as catalysis and electronics.[1–11] However, the indefinite structures (compositions) and poly-distribution of doped nanoparticles impede the in-depth investigation of the structure–property correlation, which is of interest after the very recent research in atomically mono-disperse doped nanoclusters[12–19] since their atomic structure could be resolved using unambiguous single crystal X-ray crystallography (SCXC). Early in 2009, Murray and colleagues first identified $Au_{24}Pd(SR)_{18}$ (SR: thiolate) in a mixture with $Au_{25}(SR)_{18}$ clusters using mass spectra,[20] subsequently Negish *et al.* isolated highly pure $Au_{24}Pd(SR)_{18}$ clusters using high performance liquid chromatography[21] and reported the remarkable enhancement in ligand-exchange reactivity compared with $Au_{25}(SR)_{18}$;[22] Jin and coworkers then synthesized $Au_{24}Pt(SR)_{18}$ and showed its high catalytic activity to styrene oxidation.[23] After these initial works, a few other atomically mono-disperse doped nanoclusters including $Au_{36}Pd_2(SR)_{24}$,[24] $Au_{25}Ag_2(SR)_{18}$,[25] $Au_{24}Cd(SR)_{18}$,[26] $Au_{24}Hg(SR)_{18}$,[27] $Ag_{24}Pd(SR)_{18}$,[28] $Ag_{24}Pt(SR)_{18}$,[28] and $Ag_{24}Au(SR)_{18}$[29] have been synthesized *via* various strategies, and even most of their structures have been resolved using SCXC. The X-ray structure of $Au_{24}Pd(SR)_{18}$ was obtained very recently (just before the submission of this manuscript),[30] while the $Au_{24}Pt(SR)_{18}$ structure determined using SCXC has not been reported until now, regardless of the fact that it was theoretically predicted[30,31] along with some experimental clues.[23,32] Another important issue yet to be known is how Pt or Pd doping tunes the properties of the clusters (especially the magnetism, which is complex when the sample is not of high quality, *i.e.*, traces of impurities are introduced). These questions are challenging but significant for nanocluster (even nanoparticle) research, and inspire our research enthusiasm. Fortunately, after continuous efforts we successfully resolved the atomic structures of both $Au_{24}Pd(SR)_{18}$ and $Au_{24}Pt(SR)_{18}$ recently, and found that doping with Pd or Pt turns the magnetism of neutral $Au_{25}(SR)_{18}$[33–36] from paramagnetism to diamagnetism due to the conversion of the electronic configuration. What's more, based on the known structures, it is revealed that the major magnetism of neutral $Au_{25}(SR)_{18}$ nanoclusters is distributed in its Au_{13} icosahedron kernel.

At the start of this project, $[Au_{25}(PET)_{18}]^-$ and $[Au_{25}(PET)_{18}]^0$ (PET = SCH_2CH_2Ph) were synthesized *via* the reported method.[37,38] Pd and Pt doped $Au_{25}(PET)_{18}$ nanoclusters were synthesized referring to a previous method with some modifications.[21,23,31] For the detailed synthesis and some characterizations, see ESI.† It's known that $[Au_{25}(PET)_{18}]^-$ shows three featured peaks at ~400, ~445 and ~680 nm.[39] After $[Au_{25}(PET)]^-$ is oxidized to $[Au_{25}(PET)]^0$, the ~400 nm shoulder becomes more protrudent while the ~445 nm peak becomes less so.[37] When one Pd atom is doped into a Au_{25} nanocluster, the ~400 and ~680 nm peaks obviously shift to ~375 and ~650 nm, respectively, accompanied by the feature peaks broadening, while the doping of Pt leads to a more dramatic change in the feature absorption of $Au_{25}(PET)_{18}$ nanoclusters and only two prominent peaks at ~375 and ~600 nm are observed in the UV/vis/NIR absorption spectrum, indicating that Pt-doping can more greatly tune the electronic structure of $Au_{25}(PET)_{18}$ compared to Pd-doping, similar to some previous reports.[21,23] It is of note that the UV/vis/NIR absorption spectrum of Pd (or Pt) doped $Au_{25}(PET)_{18}$ nanoclusters is also remarkably differentiated from that of $Au_{24}Cd(PET)_{18}$,[26] $Au_{24}Hg(PET)_{18}$,[27] or $Au_{25}Ag_2(PET)_{18}$[25]

[a] Key Laboratory of Materials Physics, Anhui Key Laboratory of Nanomaterials and Nanostructures, Institute of Solid State Physics, Chinese Academy of Sciences, Hefei 230031, China. E-mail: zkwu@issp.ac.cn
[b] Hefei National Laboratory for Physical Sciences at the Microscale and Synergetic Innovation Center of Quantum Information and Quantum Physics, University of Science and Technology of China, Hefei, Anhui 230026, China

† Electronic supplementary information (ESI) available: Detailed information about the MS, UV/vis/NIR spectra, 1D and 2D NMR and X-ray crystallographic analysis, and EPR signals of $[Au_{25}(SC_6H_{13})_{18}]^0$; X-ray file for $[Au_{24}Pd(PET)_{18}]^0$ (CIF); X-ray file for $[Au_{24}Pt(PET)_{18}]^0$ (CIF). CCDC 1447724 and 1447725. For ESI and crystallographic data in CIF or other electronic format see DOI: 10.1039/c6cc02698b

(see Fig. S1, ESI†), indicating that the doping can really tune the electronic structure of the matrix nanoclusters. To determine the formulas and purity of the products, matrix-assisted laser desorption ionization flight time mass spectrometry (MALDI-TOF-MS) was first employed. The intensive peak at m/z ~7303 or ~7392 in the mass spectrum indicates that the formula of the as-obtained product is $Au_{24}Pd(PET)_{18}$ or $Au_{24}Pt(PET)_{18}$, respectively, which is confirmed by the excellent agreement between the experimental and theoretical isotope patterns (Fig. S2, ESI†). The absence of a peak at ~7394 m/z excludes the existence of $Au_{25}(PET)_{18}$ and indicates the high purity of the products.

Based on the improved synthesis and purification, we successfully grew high quality $Au_{24}Pd(PET)_{18}$ and $Au_{24}Pt(PET)_{18}$ single crystals. It is of note that the yield and purity of Pd or Pt doped $Au_{25}(PET)_{18}$ nanoclusters are sensitive to the synthesis parameters (the feeding reactants ratio, aging time, *etc.*) and eventually improved after the reaction kinetics and thermodynamics[40,41] were subtly tailored (for the synthesis details, see ESI†). The solvent is also important for crystallization and it is found that the diffusion of methanol into the toluene solution is ideal for the growth of high quality single crystals of $[Au_{24}Pt(PET)_{18}]^0$ and $[Au_{24}Pd(PET)_{18}]^0$. SCXC revealed that each unit cell in the single crystals has a $Au_{24}Pd(PET)_{18}$ or $Au_{24}Pt(PET)_{18}$ nanocluster accompanied by two toluene molecules (Fig. S3 and S4 and Tables S1 and S2, ESI†). The absence of counter ions indicates the neutrality of $Au_{24}Pd(PET)_{18}$ and $Au_{24}Pt(PET)_{18}$, which is in agreement with some other characterizations.[34]

The structures of $[Au_{24}Pd(PET)_{18}]^0$ and $[Au_{24}Pt(PET)_{18}]^0$ can be briefly described as centered icosahedral $Pd@Au_{12}$ or $Pt@Au_{12}$ kernels protected by six –RS–Au–SR–Au–SR– dimeric staples (Fig. 1d–i), and have an overall framework structure similar to that of $[Au_{25}(PET)_{18}]^0$ (Fig. 1a–c) with some kernel distortion.[37] The Pt L_3-edge X-ray absorption near edge structure (XANES)[32,42–44] spectrum shows three characteristic peaks at 11 569, 11 597, and 11 623 eV, similar to those for Pt foil (see Fig. S5, ESI†), somehow implying the possible core doping of Pt in $[Au_{24}Pt(PET)_{18}]^0$. The calculated single point energies for core, inner-shell and outer-shell doped $[Au_{25}(PET)_{18}]^0$ based on the resolved structure are 0, 1.01 and 1.62 eV, respectively, indicating the core occupying of Pt in $[Au_{24}Pt(PET)_{18}]^0$ is the most energetically favorable case. Besides, the similar ^{1}H NMR splittings between $[Au_{24}Pt(PET)_{18}]^0$ and $[Au_{25}(PET)_{18}]^0$ (*vide infra*) further evidence it, since otherwise the outer-shell or inner-shell doping would break the symmetry of the ligand environment and result in totally different ^{1}H NMR splittings of $[Au_{24}Pt(PET)_{18}]^0$ compared to those of $[Au_{25}(PET)_{18}]^0$.[23] The M–Au (M: Pd or Pt) distances between the M core and the icosahedron vertex range from 2.7485 to 2.7950 Å (average: 2.7692 Å, standard deviation: 0.0204) for $[Au_{24}Pd(PET)_{18}]^0$ and from 2.7596 to 2.7978 Å (average: 2.7781 Å, standard deviation: 0.0154) for $[Au_{24}Pt(PET)_{18}]^0$, which are a little shorter and more deviated than those of $[Au_{25}(PET)_{18}]^0$ nanoclusters (average: 2.7867 Å, standard deviation: 0.0090), indicating the doping-induced Jahn–Teller effect,[31,36] which is further illustrated by the following comparisons: the Au–Au distances of the Au_{12} cage in the Au_{13} icosahedron range from 2.7347 to 3.1974 Å (average: 2.9123 Å, standard deviation: 0.1659) and from 2.7426 to 3.2078 Å (average: 2.9212 Å, standard deviation: 0.1606) for $[Au_{24}Pd(PET)_{18}]^0$ and $[Au_{24}Pt(PET)_{18}]^0$, respectively, which are more deviated than those of $[Au_{25}(PET)_{18}]^0$ nanoclusters (average: 2.9138 Å, standard deviation: 0.0895); the Pd(Pt)–Au distances between the core and the outer-shell gold atom range from 4.7873 to 5.0132 Å (average: 4.8925 Å, standard deviation: 0.0843) and from 4.7999 to 5.0347 Å (average: 4.9121 Å, standard deviation: 0.0899), respectively, which are also more deviated than the distances between the core and the outer-shell gold atom (average: 4.8914 Å, standard deviation: 0.0318) in $[Au_{25}(PET)_{18}]^0$ nanoclusters. Overall, $[Au_{24}Pd(PET)_{18}]^0$ and $[Au_{24}Pt(PET)_{18}]^0$ remain in the framework structure of $[Au_{25}(PET)_{18}]^0$ (Fig. 1a–c) with some Jahn–Teller-like distortion, which is very similar to a previous theoretical calculation.[31]

Magnetism makes gold nanoparticles (nanoclusters) more attractive,[45–48] however, magnetism can always be complex by the introduction of traces of impurities and the magnetism of $[Au_{24}Pd(PET)_{18}]^0$ and $[Au_{24}Pt(PET)_{18}]^0$ has not been previously reported to the best of our knowledge. Based on the high quality samples, we can accurately evaluate the intrinsic magnetism of $[Au_{24}Pd(PET)_{18}]^0$ and $[Au_{24}Pt(PET)_{18}]^0$. Electron paramagnetic resonance (EPR) spectroscopy shows that both $[Au_{24}Pd(PET)_{18}]^0$ and $[Au_{24}Pt(PET)_{18}]^0$ are diamagnetic (Fig. 2), while $[Au_{25}(PET)_{18}]^0$ is paramagnetic (which is also similar to previous reports[33–36]), indicating that the center doping by Pd or Pt induces the magnetism turn-off of $[Au_{25}(PET)_{18}]^0$. It is known that both

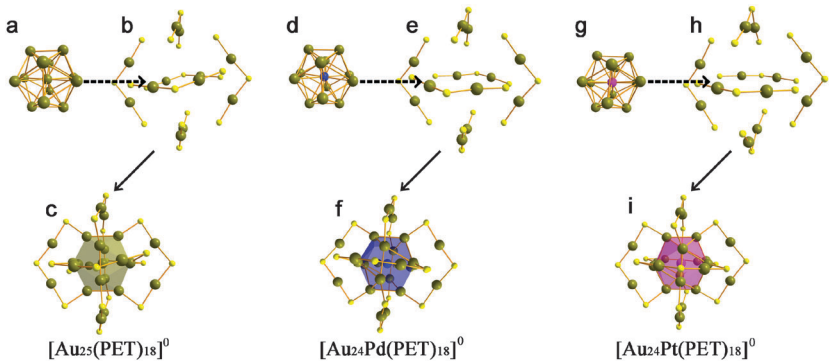

Fig. 1 Structure anatomy of $[Au_{25}(PET)_{18}]^0$ (c), $Au_{24}Pd(PET)_{18}$ (f) and $Au_{24}Pt(PET)_{18}$ (i). (a), (d) or (g): kernel; (b), (e) or (h): outer shell.

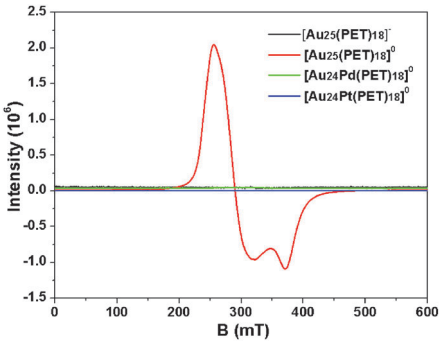

Fig. 2 EPR signals of $[Au_{25}(PET)_{18}]^-$ (black), $[Au_{25}(PET)_{18}]^0$ (red), $[Au_{24}Pd(PET)_{18}]^0$ (green) and $[Au_{24}Pt(PET)_{18}]^0$ (blue).

$[Au_{24}Pd(PET)_{18}]^0$ and $[Au_{24}Pt(PET)_{18}]^0$ have superatomic 6-electron configurations, while $[Au_{25}(PET)_{18}]^0$ bears a 7-electron configuration, thus the magnetism turning from paramagnetism ($[Au_{25}(PET)_{18}]^0$) to diamagnetism ($[Au_{24}Pd(PET)_{18}]^0$ or $[Au_{24}Pt(PET)_{18}]^0$) is probably caused by electron configuration conversion, which is supported by the fact that when 7-electron configured $[Au_{25}(PET)_{18}]^0$ transforms to 6-electron configured $[Au_{25}(PET)_{18}]^+$ or 8-electron configured $[Au_{25}(PET)_{18}]^-$, the magnetism turns from paramagnetic to diamagnetic,[36,49] too.

Following the magnetism origin issue, another intriguing issue is where the major paramagnetism locates, the Au_{13} icosahedron or the surface staples of the $Au_{25}(SR)_{18}$ system. A previous theoretical calculation revealed that the Au_{13} icosahedron was the major magnetism source,[33,34] but experimental evidence has not been presented so far. It is challenging to separately measure the magnetism of the kernel and the surface motifs. However, the atomic structure unraveling of both $[Au_{24}Pd(PET)_{18}]^0$ and $[Au_{24}Pt(PET)_{18}]^0$ provides a chance to clarify it in some indirect way.

Previously, it was found that the two Au–S binding modes in $Au_{25}(PET)_{18}$ nanoclusters can echo the chemical shifts (CSs) of the connected methene protons[50–55] (*i.e.* the methene protons adjacent to the icosahedron or the surface gold have remarkably different CSs). It is also found that the magnetism has some influence on the CSs of the above mentioned two kinds of methene protons,[50,53,55] thus it is possible to determine the main source of magnetism in neutral $[Au_{25}(PET)_{18}]^0$ from the NMR results. To facilitate the interpretation, the subscripts "in" and "out" are used to label the resonances of 12 inner ligands and 6 outer ligands in the nanocluster, respectively, and the "α" or "β" position is named relative to the S atom in the ligand (Fig. S6, ESI†). First, the peaks in the NMR spectra are well assigned based on the 1D and 2D NMR results (Fig. S7–S12, ESI†) as well as some previous works.[23,50–55] For $[Au_{25}(PET)_{18}]^-$, the triplet peak at 2.93 ppm pertains to $(\beta\text{-CH}_2)_{out}$, and the complex peak centered at 3.21 ppm is due to the overlap of the $(\alpha\text{-CH}_2)_{out}$ and $(\beta\text{-CH}_2)_{in}$ resonances.[50] The remaining broad peak at 4.53 ppm is thus assigned to $(\alpha\text{-CH}_2)_{in}$ (Fig. S7a and S8a, ESI†).[50] Compared with those in $[Au_{25}(PET)_{18}]^-$, the $(\alpha\text{-CH}_2)_{out}$ and $(\beta\text{-CH}_2)_{in}$ resonances in $[Au_{25}(PET)_{18}]^0$ shift downfield from 3.21 to 5.10 ppm, while the $(\alpha\text{-CH}_2)_{in}$ resonances undergo a downfield shift from 4.53 to 23.6 ppm (Fig. S7b, S8b, and S10, and Table S1, ESI†), similar to in a previous report.[50] It is of note that the $(\alpha\text{-CH}_2)_{in}$ signals are not observed in the usual ^{1}H NMR spectral window, neither by increasing or decreasing the temperature, and it is even barely detectable and very broad at 298 K, as reported by Maran and co-workers.[50] Upon increasing the temperature, the peak sharpens and can be clearly observed (Fig. S9, ESI†). To evaluate the charge state interference of $[Au_{25}(PET)_{18}]^0$, the NMR spectra of neutral $[Au_{24}Pd(PET)_{18}]^0$ and $[Au_{24}Pt(PET)_{18}]^0$ were measured and are shown in Fig. S7 (ESI†). In these two cases, the $(\alpha\text{-CH}_2)_{in}$ peaks locate at 3.51 and 3.88 ppm, respectively (Fig. S7c–d, S8c–d, S11 and S12, ESI†), these exclude the charge stage influence of $[Au_{25}(PET)_{18}]^0$ and even indicates that the composition of the core doesn't greatly influence the $(\alpha\text{-CH}_2)_{in}$ resonances. $[Au_{24}Pd(PET)_{18}]^0$ and $[Au_{24}Pt(PET)_{18}]^0$ nanoclusters are diamagnetic, as revealed by EPR (Fig. 2), and they have a similar structure to $[Au_{25}(PET)_{18}]^0$ as discussed above. Thus, the surprising downshift of the $(\alpha\text{-CH}_2)_{in}$ signals should be caused by the magnetism of $[Au_{25}(PET)_{18}]^0$, as indicated in previous works.[50,53,55] In particular, the greater downshift of $(\alpha\text{-CH}_2)_{in}$ resonances compared with those of $(\alpha\text{-CH}_2)_{out}$ signals indicates that the magnetism (at least the major magnetism) comes from the Au_{13} icosahedron of $[Au_{25}(PET)_{18}]^0$, because the $(\alpha\text{-CH}_2)_{in}$ closely connects with the Au_{13} icosahedron while the $(\alpha\text{-CH}_2)_{out}$ is more adjacent to the outer-shell gold atoms. The almost equal downshift of the $(\beta\text{-CH}_2)_{in}$ and $(\alpha\text{-CH}_2)_{out}$ peaks supports this conclusion since the magnetic field influence is distance-sensitive and $(\beta\text{-CH}_2)_{in}$ and $(\alpha\text{-CH}_2)_{out}$ have close spacings to the Au_{13} icosahedron. On the other hand, the unchanged EPR results (including the intensity and the profile, Fig. S13, ESI†) after the phenylethanolate was replaced by hexanethiolate in $[Au_{25}(SR)_{18}]^0$ also indicate that the surface ligands have little contribution to the magnetism of $[Au_{25}(SR)_{18}]^0$. Taken together, our experiments demonstrate that the paramagnetism of $[Au_{25}(SR)_{18}]^0$ primarily distributes in the Au_{13} kernel, verifying the rationality of the previous theoretical calculation.[33]

In summary, we have grown high quality single crystals of $[Au_{24}Pd(PET)_{18}]^0$ and $[Au_{24}Pt(PET)_{18}]^0$ *via* an improved synthesis and purification, successfully resolved the atomic structures of $[Au_{24}Pd(PET)_{18}]^0$ and $[Au_{24}Pt(PET)_{18}]^0$ using SCXC, discovered that the mono-Pt or mono-Pd doping leads to the magnetism of $[Au_{25}(PET)_{18}]^0$ turning from paramagnetism to diamagnetism, and experimentally demonstrated that the Au_{13} icosahedron is the major magnetism location for $[Au_{25}(PET)_{18}]^0$ in comparison with the surface motifs.

This work was supported by Natural Science Foundation of China (numbers 21222301, 21528303 and 21171170), the Innovative Program of Development Foundation of Hefei Center for Physical Science and Technology (2014FXCX002), Hefei Science Center, CAS (user of potential: 2015HSC-UP003), and the CAS/SAFEA International Partnership Program for Creative Research Teams with financial support. The calculations were conducted on the supercomputing system in the Supercomputing Center of University of Science and Technology of China. We greatly thank High Magnetic Field Laboratory (HMFL), Chinese Academy of Sciences for EPR and NMR measurements.

Notes and references

1 T. Shibata, B. A. Bunker, Z. Zhang, D. Meisel, C. F. Vardeman and J. D. Gezelter, *J. Am. Chem. Soc.*, 2002, **124**, 11989–11996.
2 R. Ferrando, J. Jellinek and R. L. Johnston, *Chem. Rev.*, 2008, **108**, 845–910.
3 W. Liang, B. D. Yuhas and P. Yang, *Nano Lett.*, 2009, **9**, 892–896.
4 Q. B. Zhang, J. P. Xie, J. Liang and J. Y. Lee, *Adv. Funct. Mater.*, 2009, **19**, 1387–1398.
5 D. S. Wang and Y. D. Li, *Adv. Mater.*, 2011, **23**, 1044–1060.
6 F. Gao and D. W. Goodman, *Chem. Soc. Rev.*, 2012, **41**, 8009–8020.
7 X. Dou, X. Yuan, Q. Yao, Z. Luo, K. Zheng and J. Xie, *Chem. Commun.*, 2014, **50**, 7459–7462.
8 X. Dou, X. Yuan, Y. Yu, Z. Luo, Q. Yao, D. T. Leong and J. Xie, *Nanoscale*, 2014, **6**, 157–161.
9 N. Zhang, X. Chen, Y. Lu, L. An, X. Li, D. Xia, Z. Zhang and J. Li, *Small*, 2014, **10**, 2662–2669.
10 C. Hao, L. Xu, W. Ma, X. Wu, L. Wang, H. Kuang and C. Xu, *Adv. Funct. Mater.*, 2015, **25**, 5816–5822.
11 X. Wang, S.-I. Choi, L. T. Roling, M. Luo, C. Ma, L. Zhang, M. Chi, J. Liu, Z. Xie, J. A. Herron, M. Mavrikakis and Y. Xia, *Nat. Commun.*, 2015, **6**, 7594.
12 J.-H. Jia, J.-X. Liang, Z. Lei, Z.-X. Cao and Q.-M. Wang, *Chem. Commun.*, 2011, **47**, 4739–4741.
13 T. Udayabhaskararao, Y. Sun, N. Goswami, S. K. Pal, K. Balasubramanian and T. Pradeep, *Angew. Chem., Int. Ed.*, 2012, **51**, 2155–2159.
14 H. Y. Yang, Y. Wang, H. Q. Huang, L. Gell, L. Lehtovaara, S. Malola, H. Hakkinen and N. F. Zheng, *Nat. Commun.*, 2013, **4**, 2422.
15 H. Y. Yang, Y. Wang, J. Lei, L. Shi, X. H. Wu, V. Makinen, S. C. Lin, Z. C. Tang, J. He, H. Hakkinen, L. S. Zheng and N. F. Zheng, *J. Am. Chem. Soc.*, 2013, **135**, 9568–9571.
16 C. Kumara, C. M. Aikens and A. Dass, *J. Phys. Chem. Lett.*, 2014, **5**, 461–466.
17 N. Bhattarai, D. M. Black, S. Boppidi, S. Khanal, D. Bahena, A. Tlahuice-Flores, S. B. H. Bach, R. L. Whetten and M. Jose-Yacaman, *J. Phys. Chem. C*, 2015, **119**, 10935–10942.
18 C. Kumara, K. J. Gagnon and A. Dass, *J. Phys. Chem. Lett.*, 2015, **6**, 1223–1228.
19 S. Wang, S. Jin, S. Yang, S. Chen, Y. Song, J. Zhang and M. Zhu, *Sci. Adv.*, 2015, **1**, e1500441.
20 C. A. Fields-Zinna, M. C. Crowe, A. Dass, J. E. F. Weaver and R. W. Murray, *Langmuir*, 2009, **25**, 7704–7710.
21 Y. Negishi, W. Kurashige, Y. Niihori, T. Iwasa and K. Nobusada, *Phys. Chem. Chem. Phys.*, 2010, **12**, 6219–6225.
22 Y. Niihori, W. Kurashige, M. Matsuzaki and Y. Negishi, *Nanoscale*, 2013, **5**, 508–512.
23 H. Qian, D.-e. Jiang, G. Li, C. Gayathri, A. Das, R. R. Gil and R. Jin, *J. Am. Chem. Soc.*, 2012, **134**, 16159–16162.
24 N. Barrabés, B. Zhang and T. Burgi, *J. Am. Chem. Soc.*, 2014, **41**, 14361–14364.
25 C. Yao, J. Chen, M. B. Li, L. Liu, J. Yang and Z. Wu, *Nano Lett.*, 2015, **15**, 1281–1287.
26 C. Yao, Y. J. Lin, J. Yuan, L. Liao, M. Zhu, L. H. Weng, J. Yang and Z. Wu, *J. Am. Chem. Soc.*, 2015, **137**, 15350–15353.
27 L. Liao, S. Zhou, Y. Dai, L. Liu, C. Yao, C. Fu, J. Yang and Z. Wu, *J. Am. Chem. Soc.*, 2015, **137**, 9511–9514.
28 J. Yan, H. Su, H. Yang, S. Malola, S. Lin, H. Hakkinen and N. Zheng, *J. Am. Chem. Soc.*, 2015, **137**, 11880–11883.
29 M. S. Bootharaju, C. P. Joshi, M. R. Parida, O. F. Mohammed and O. M. Bakr, *Angew. Chem., Int. Ed.*, 2016, **3**, 922–927.
30 M. A. Tofanelli, T. W. Ni, B. D. Phillips and C. J. Ackerson, *Inorg. Chem.*, 2016, **55**, 999–1001.
31 K. Kwak, Q. Tang, M. Kim, D. E. Jiang and D. Lee, *J. Am. Chem. Soc.*, 2015, **137**, 10833–10840.
32 S. L. Christensen, M. A. MacDonald, A. Chatt, P. Zhang, H. Qian and R. Jin, *J. Phys. Chem. C*, 2012, **116**, 26932–26937.
33 M. Z. Zhu, C. M. Aikens, M. P. Hendrich, R. Gupta, H. F. Qian, G. C. Schatz and R. C. Jin, *J. Am. Chem. Soc.*, 2009, **131**, 2490–2492.
34 S. Antonello, N. V. Perera, M. Ruzzi, J. A. Gascon and F. Maran, *J. Am. Chem. Soc.*, 2013, **135**, 15585–15594.
35 K. S. Krishna, P. Tarakeshwar, V. Mujica and C. S. Kumar, *Small*, 2014, **10**, 907–911.
36 M. A. Tofanelli, K. Salorinne, T. W. Ni, S. Malola, B. Newell, B. Phillips, H. Häkkinen and C. J. Ackerson, *Chem. Sci.*, 2016, **7**, 1882–1890.
37 M. Zhu, W. T. Eckenhoff, T. Pintauer and R. Jin, *J. Phys. Chem. C*, 2008, **112**, 14221–14224.
38 Z. Wu, J. Suhan and R. Jin, *J. Mater. Chem.*, 2009, **19**, 622–626.
39 M. Zhu, C. M. Aikens, F. J. Hollander, G. C. Schatz and R. Jin, *J. Am. Chem. Soc.*, 2008, **130**, 5883–5885.
40 Z. Wu, M. A. MacDonald, J. Chen, P. Zhang and R. Jin, *J. Am. Chem. Soc.*, 2011, **133**, 9670–9673.
41 X. Yuan, B. Zhang, Z. Luo, Q. Yao, D. T. Leong, N. Yan and J. Xie, *Angew. Chem., Int. Ed.*, 2014, **53**, 4623–4627.
42 Y. Negishi, W. Kurashige, Y. Kobayashi, S. Yamazoe, N. Kojima, M. Seto and T. Tsukuda, *J. Phys. Chem. Lett.*, 2013, **4**, 3579–3583.
43 Y. Li, H. Cheng, T. Yao, Z. Sun, W. Yan, Y. Jiang, Y. Xie, Y. Sun, Y. Huang, S. Liu, J. Zhang, Y. Xie, T. Hu, L. Yang, Z. Wu and S. Wei, *J. Am. Chem. Soc.*, 2012, **134**, 17997–18003.
44 L. Yang, H. Cheng, Y. Jiang, T. Huang, J. Bao, Z. Sun, Z. Jiang, J. Ma, F. Sun, Q. Liu, T. Yao, H. Deng, S. Wang, M. Zhu and S. Wei, *Nanoscale*, 2015, **7**, 14452–14459.
45 P. Crespo, R. Litran, T. C. Rojas, M. Multigner, J. M. de la Fuente, J. C. Sanchez-Lopez, M. A. Garcia, A. Hernando, S. Penades and A. Fernandez, *Phys. Rev. Lett.*, 2004, **93**, 087204.
46 Y. Negishi, H. Tsunoyama, M. Suzuki, N. Kawamura, M. M. Matsushita, K. Maruyama, T. Sugawara, T. Yokoyama and T. Tsukuda, *J. Am. Chem. Soc.*, 2006, **128**, 12034–12035.
47 J. de la Venta, A. Pucci, E. Fernandez Pinel, M. A. Garcia, C. De Julian Fernandez, P. Crespo, P. Mazzoldi, G. Ruggeri and A. Hernando, *Adv. Mater.*, 2007, **19**, 875–877.
48 Z. Wu, J. Chen and R. Jin, *Adv. Funct. Mater.*, 2011, **21**, 177–183.
49 D.-e. Jiang and S. Dai, *Inorg. Chem.*, 2009, **48**, 2720–2722.
50 A. Venzo, S. Antonello, J. A. Gascon, I. Guryanov, R. D. Leapman, N. V. Perera, A. Sousa, M. Zamuner, A. Zanella and F. Maran, *Anal. Chem.*, 2011, **83**, 6355–6362.
51 J. F. Parker, J. P. Choi, W. Wang and R. W. Murray, *J. Phys. Chem. C*, 2008, **112**, 13976–13981.
52 Z. K. Wu, C. Gayathri, R. R. Gil and R. C. Jin, *J. Am. Chem. Soc.*, 2009, **131**, 6535–6542.
53 S. Antonello, G. Arrigoni, T. Dainese, M. De Nardi, G. Parisio, L. Perotti, A. Rene, A. Venzo and F. Maran, *ACS Nano*, 2014, **8**, 2788–2795.
54 T. Dainese, S. Antonello, J. A. Gascon, F. Pan, N. V. Perera, M. Ruzzi, A. Venzo, A. Zoleo, K. Rissanen and F. Maran, *ACS Nano*, 2014, **8**, 3904–3912.
55 M. De Nardi, S. Antonello, D. E. Jiang, F. Pan, K. Rissanen, M. Ruzzi, A. Venzo, A. Zoleo and F. Maran, *ACS Nano*, 2014, **8**, 8505–8512.

